Theoretical prediction of the onset of thermal instability in the thermal entrance region of horizontal rectangular channels

J. N. Lin
Department of System Engineering, Chung-Cheng Institute of Technology, Tashi, Taiwan, ROC

F. C. Chou
Department of Mechanical Engineering, National Central University, Chung-Li, Taiwan, ROC

P. Y. Tzeng
Department of Aeronautical Engineering, Chung-Cheng Institute of Technology, Tashi, Taiwan, ROC

A numerical analysis was performed to study the onset of thermal instability in the thermal entrance region of horizontal rectangular ducts. Three kinds of surface thermal boundary conditions are considered. In the analysis, three dimensionless groups, namely, Rayleigh number Ra, aspect ratio γ, and Prandtl number Pr appear. Their corresponding influences on the local Nusselt number distributions and the onset of thermal instability are investigated. The predicted results, based on the criterion of 2% deviation of the local Nusselt number from that of Graetz theory, are in agreement with the published experimental data. Results show that the thermal instability is only slightly affected by the change of γ under fixed Pr for the thermal condition of case 1 (the bottom wall is heated while the top wall is cooled and the side walls are adiabatic) and of case 2 (heated from below while the other walls are insulated), while for the isothermal channels (case 3), the effects of different γ on the instability become significant. Another criterion, based on the location of the minimum local Nusselt number, is also considered in order to investigate the effects of the selection of different criteria on the prediction of the onset of thermal instability.

Keywords: thermal instability; mixed convection; thermal entrance region

Introduction

The flow and heat transfer characteristics of laminar forced convection are significantly affected by buoyancy-induced secondary flow. Thus, the effect of buoyancy force on laminar forced-convective flows with various geometrical shapes has been studied by many investigators in recent years because of its theoretical interest and practical significance. Notable examples include the applications in the design of heat exchangers, nuclear reactors, and channel-type solar energy collectors. The buoyancy effect is particularly pronounced for horizontal ducts, where it may act to enhance heat transfer and induce early transition to turbulence. The precursor to the effect is a thermal instability that results in the development of longitudinal vortex rolls. Hence, to establish the existence of the buoyancy effect, conditions marking the onset of thermal instability must be known. A linear stability analysis is usually used to determine the onset of longitudinal vortex rolls between two horizontal parallel plates[1–3] and along a horizontal flat plate.[4]

To verify the predictions, Akiyama et al.,[5] Hwang and Liu,[6] and Kamotani et al.[7] visualized air flow in horizontal parallel-plate channels heated from below. A single stream of dye was injected along the midline of the bottom plate, and a side view was used to determine the longitudinal station at which buoyancy force causes the dye to ascend or descend from the plate. Kamotani and Ostrach[8] also performed experiments for air flow in the thermal entrance region of a rectangular channel and determined the onset of the thermal instability by detecting small spanwise temperature variations. It is noteworthy that the measured values of the critical Rayleigh number exceeded predictions by more than an order of magnitude. A similar study was also experimentally performed by Incropera and his coworkers[9] for water flow in the thermal entrance region of a horizontal duct. Correlations for the critical Rayleigh number, which are determined by the criterion of 10% departure of local Nusselt number from the forced-convection results,[10] or by flow visualization and the occurrence of a minimum local Nusselt number,[9] are found to be a function of the Graetz number. Recently, experiments on mixed convection for airflow in a horizontal and inclined channel were carried out by Maughan and Incropera[11] to study the onset of thermal instability. The departure of the spanwise-average longitudinal Nusselt number from the forced-convection results was used to mark the onset point.

Instead of the conventional linear stability theory, the finite-difference solution of Navier–Stokes and energy equations has been used to investigate the thermal instability. However, the published works are rather too limited to consider or discuss the effects of different parameters on the thermal instability and are unable to predict accurately the relation of critical Rayleigh number versus the critical axial distance z for onset of thermal

Address reprint requests to Dr. Chou at the Department of Mechanical Engineering, National Central University, Chung-Li, Taiwan 32054, Republic of China.

Received 5 June 1990; accepted 26 November 1990

instability. The numerical solution was obtained by Ou et al.[12] for large Prandtl number fluids in a rectangular isothermal duct. In their analysis, the 2% deviation of local Nusselt number from the value for pure forced convection was used as the criterion for onset of the secondary flow. Compared to the experimental data, it suggested earlier onset of thermal instability by about an order of magnitude. The onset of thermally driven secondary flow in horizontal rectangular ducts was also studied numerically for water flow in the combined and thermal entrance regions for different surface thermal conditions and aspect ratio.[10] The onset of secondary flow is ascribed to an occurrence of reduction in bottom-plate temperature near the side wall, which is due to buoyancy-driven upward motion of warm fluid along the side wall and a descending motion of adjoining cooler fluid. The predictions of the critical Rayleigh number for the thermal entry region also exceeded the measured values by about an order of magnitude. There are also other previous works concerning laminar mixed convection in the entrance region of horizontal ducts.[13–19]

The present article shows a systematic theoretical study on laminar mixed convection in the thermal entrance region of horizontal rectangular channels. A 2% deviation of the local Nusselt number from the value for pure forced convection is used as the criterion for the prediction of the onset of thermal instability. The specific effects such as Prandtl number, aspect ratio, and side-wall heating are also considered. Finally, a comparison between results based on the criterion of a 2% deviation of local Nusselt number and that based on the occurrence of minimum local Nusselt number are made to study the influence of selection of this criterion.

Theoretical methods

The channel flow, which is shown in Figure 1, is three-dimensional (3-D) and is characterized by velocity components u, v, and w in the spanwise x-, vertical y-, and longitudinal z-directions, respectively. The viscous dissipation and compressibility effects in the energy equation are neglected. The Boussinesq approximation is used to characterize the buoyancy effect. By introducing the dimensionless variables and parameters

$$\begin{aligned} &x=X/D_e,\quad y=Y/D_e,\quad z=Z/[\mathrm{Pr}\,\mathrm{Re}\,D_e],\quad u=U/U_c,\\ &v=V/U_c,\quad w_f=W_f/\bar{W}_f,\quad w=W/[\mathrm{Ra}\,\bar{W}_f],\\ &\theta=[T-T_r]/[T_h-T_c]\ \text{(for case 1)},\quad T_r=(T_h+T_c)/2,\\ &\theta=[T-T_w]/\theta_c\ \text{(for cases 2 and 3)},\\ &p=P/[\rho U_c v/D_e],\quad \mathrm{Gr}=g\beta\theta_c D_e^3/v^2,\quad \mathrm{Pr}=v/\alpha,\\ &\mathrm{Ra}=\mathrm{PrGr},\quad \mathrm{Re}=\bar{W}_f D_e/v,\quad \mathrm{Pe}=\mathrm{PrRe} \end{aligned} \tag{1}$$

where $D_e=4A/S$, $U_c=\mathrm{Gr}v/D_e$, and $\theta_c=T_0-T_w$, the dimensionless governing equations can be obtained. By introducing a vorticity function in the axial directions, the vorticity-velocity formulation of the Navier–Stokes equations is employed to describe the mixed convection heat transfer in a horizontal duct.[18] The governing equations then become

$$\nabla^2 u=\frac{\partial \xi}{\partial y}-\frac{\partial^2 w}{\partial x\,\partial z} \tag{2}$$

Notation

A	Cross-sectional area of a channel (m^2)
a, b	Width and height of a rectangular channel, respectively
C	Constant, $-(D_e^2/\mu\bar{W}_f)\,\partial P_f/\partial Z$
D_e	Equivalent hydraulic diameter, $4A/S$ (m)
f	Friction factor, $2\bar{\tau}_w/(\rho\bar{W}'^2)$
g	Gravitational acceleration (m/s^2)
Gr	Grashof number, $g\beta\theta_c D_e^3/v^2$
$\bar{h}$	Average heat transfer coefficient ($W/m^2\cdot K$)
k	Thermal conductivity ($W/m\cdot K$)
M, N	Number of divisions in the x- and y-directions, respectively
n	Outward normal direction to the wall
Nu	Local Nusselt number, $\bar{h}D_e/k$
Nu_1	The Nusselt number of the bottom plate
Nu_2	The Nusselt number of the top plate
P, P_f	Pressure deviation and pressure for fully developed laminar flow before thermal entrance, respectively
p	Dimensionless quantity for P
$\bar{P}$	Mean pressure averaged over the passage cross section
Pe	Peclet number, PrRe
Pr	Prandtl number, v/α
Ra	Rayleigh number, PrGr
Ra_c	Critical Rayleigh number (see Equation 13)
Re	Reynolds number, $\bar{W}_f D_e/v$
S	Circumference of cross section
T	Temperature
T_c	Surface temperature of the cooled plate
T_h	Surface temperature of the heated plate
T_0	Uniform fluid temperature at entrance
U, V	Velocity components in x-, y-directions
u, v	Dimensionless quantities for U, V
W	Perturbation of axial velocity from its value at $Z=0$
w	Dimensionless quantities for W
W_f	Fully developed axial velocity before thermal entrance
w_f	Dimensionless quantity for W_f
W'	Axial velocity in the thermal entrance region, W_f+W
w'	Dimensionless axial velocity, $w_f+\mathrm{Ra}\cdot w$
X, Y, Z	Rectangular coordinate
x, y, z	Dimensionless rectangular coordinates

Greek letters

α	Thermal diffusivity (m^2/s)
β	Coefficient of thermal expansion (K^{-1})
γ	Aspect ratio of a rectangular channel, a/b
θ	Dimensionless temperature, $(T-T_w)/\theta_c$
μ	Viscosity ($kg/m\cdot s$)
τ_w	Shear stress (N/m^2)
v	Kinematic viscosity (m^2/s)
ξ	Dimensionless vorticity in axial direction
ρ	Density (kg/m^3)

Subscripts

c	Characteristic quantity
f	Fully developed quantity before thermal entrance
w	Value at wall
0	Condition for purely forced convection

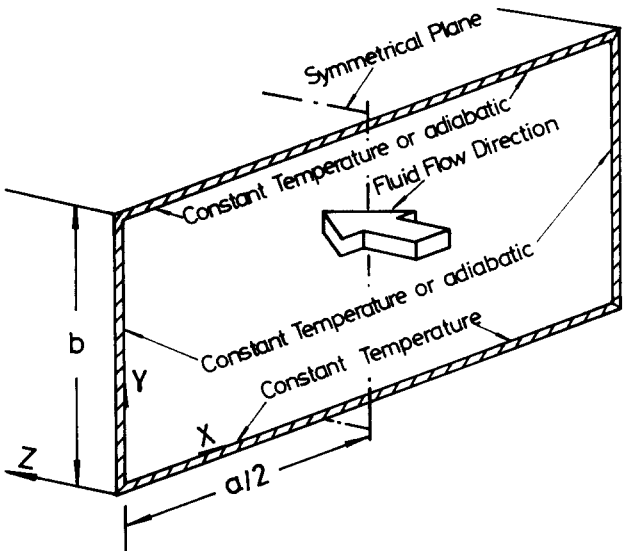

Figure 1 Flow in a horizontal rectangular channel

$$\nabla^2 v = -\frac{\partial \xi}{\partial x} - \frac{\partial^2 w}{\partial y\,\partial z} \tag{3}$$

$$\mathrm{Gr}\left(u\frac{\partial \xi}{\partial x} + v\frac{\partial \xi}{\partial y} + w\frac{\partial \xi}{\partial z} + \xi\frac{\partial u}{\partial x} + \xi\frac{\partial v}{\partial y} + \frac{\partial w}{\partial y}\right.$$

$$\left.\frac{\partial u}{\partial z} - \frac{\partial w}{\partial x}\frac{\partial v}{\partial z}\right) + \frac{1}{\mathrm{Pr}}\left(\frac{\partial w_f}{\partial y}\frac{\partial u}{\partial z} - \frac{\partial w_f}{\partial x}\frac{\partial v}{\partial z} + w_f\frac{\partial \xi}{\partial z}\right) = \nabla^2\xi - \frac{\partial \theta}{\partial x} \tag{4}$$

$$\mathrm{Gr}\left(u\frac{\partial w}{\partial x} + v\frac{\partial w}{\partial y} + w\frac{\partial w}{\partial z}\right) + \frac{1}{\mathrm{Pr}}\left(u\frac{\partial w_f}{\partial x} + v\frac{\partial w_f}{\partial y} + w_f\frac{\partial w}{\partial z}\right)$$

$$= -\frac{1}{\mathrm{Pe}^2}\frac{\partial \bar{p}}{\partial z} + \nabla^2 w \tag{5}$$

$$\nabla^2 w_f = C \tag{6}$$

$$\mathrm{Ra}\left(u\frac{\partial \theta}{\partial x} + v\frac{\partial \theta}{\partial y} + w\frac{\partial \theta}{\partial w}\right) + w_f\frac{\partial \theta}{\partial z} = \nabla^2\theta \tag{7}$$

where $\xi = \partial u/\partial y - \partial v/\partial x$ is the axial vorticity, $\nabla^2 = \partial^2/\partial x^2 + \partial^2/\partial y^2$, and $C = -(D_e^2/\mu W_f)\,\partial P_f/\partial Z = \text{constant}$. In the foregoing equations the axial diffusion effect is already neglected under the high Peclet number assumption as employed in the previous works on thermal instability by Incropera et al.,[9] Ou et al.,[12] and other previous numerical studies on laminar mixed convection in the entrance region of ducts.[14–16,18,20]

In the present study, three kinds of surface thermal conditions are considered to study the effect of side-wall heating on the onset of thermal instability. In case 1, the channel is heated from the bottom wall, while the top one is cooled and the side walls are subjected to an adiabatic conditions. The onset of thermal instability for this kind of surface thermal condition has been studied experimentally.[6,8,10,16] Incropera and his coworkers[9,16] showed that the onset of the thermal instability was independent of the upper horizontal surface thermal condition. In case 2, the thermal boundary condition is the same as that of case 1 except that a top adiabatic wall is considered rather than a cooled wall. In case 3, an isothermal channel is considered like that in Ou et al.[12] A uniform inlet fluid temperature is prescribed for all cases.

Because of symmetry, only half of the channel region is considered. The boundary conditions are

$$\begin{aligned}
&z=0\text{: } u=v=w=\xi=0, \quad \theta=-1/2 \text{ (for case 1)}\\
&\qquad\qquad \theta=0 \text{ (for cases 2 and 3)}\\
&y=0\text{: } \theta=1/2 \text{ (for case 1)}, \quad \theta=0 \text{ (for cases 2 and 3)}\\
&y=(1+\gamma)/2\gamma\text{: } \theta=-1/2 \text{ (for case 1)}\\
&\qquad\qquad \partial\theta/\partial y=0 \text{ (for case 2)}\\
&\qquad\qquad \theta=0 \text{ (for case 3)}\\
&x=0\text{: } \partial\theta/\partial x=0 \text{ (for cases 1 and 2)}, \quad \theta=0 \text{ (for case 3)}\\
&x=(1+\gamma)/4\text{: } u=\partial v/\partial x=\partial w/\partial x=\partial w_f/\partial x=\partial\theta/\partial x=0
\end{aligned} \tag{8}$$

After the developing velocity and temperature fields are obtained, the computations of the local Nusselt number are of practical and theoretical interest. In case 1, the local Nusselt numbers along the bottom and top walls are defined as in Cheng and Ou:[19]

$$\mathrm{Nu}_1 = (\overline{\partial\theta/\partial y})/(\theta_b - 1/2) \tag{9}$$

$$\mathrm{Nu}_2 = (\overline{\partial\theta/\partial y})/(\theta_b + 1/2) \tag{10}$$

The subscripts 1 and 2 denote the bottom and top walls, respectively. In case 2, the local Nusselt number $\mathrm{Nu} = \bar{h}D_e/k$ along the bottom plate can be defined as

$$\mathrm{Nu} = [(1+\gamma)(\overline{\partial(w'\theta)/\partial z})]/[2\gamma(1-\theta_b)] \tag{11}$$

In case 3, the Nusselt number can be evaluated by considering the overall energy balance for the longitudinal length dz as presented in Ou et al.[12]

$$\mathrm{Nu} = (\overline{\partial(w'\theta)/\partial z})/4[\overline{w'(\theta_w - \theta_b)}] \tag{12}$$

Simpson's rule is used to compute the average quantities indicated above.

The computation procedures for the simultaneous solutions of Equations 2–7 are similar to those in ref. 18. Since a step change in wall temperature is imposed at the entrance $z=0$ in the present work, an oscillatory behavior of local Nusselt number may arise in the region near the entrance when $z \leqq 10^{-3}$.[21] This undesired oscillation can be avoided by using a small axial step size Δz and a simple forward difference for the axial derivative terms at the left-hand side of Equations 4, 5, and 7. After considerable numerical experiments, an axial step size Δz ranging from 10^{-6} near the entrance to 3.2×10^{-5} near the fully developed region was found to be satisfactory. The cross-sectional mesh size $M\times N = 70\times28$, 90×12, and 60×12 was used for cases 1, 2, and 3, respectively. The number of axial steps is about 18,000 and the average required computing time is 3600 CPU seconds on a VAX-8650 computer.

Results and discussion

To ensure the accuracy of the present numerical results, a numerical experiment with uniform spaced grids was made on the mesh size $M\times N$ and axial step size Δz. Table 1 shows the results of local Nusselt number Nu by using different grid arrangements at some selected axial locations for case 1 with $\mathrm{Pr}=0.7$, $\mathrm{Ra}=10^5$, and $\gamma=10$. It is seen in Table 1 that the maximum deviations of Nu between $M\times N(\Delta z) = 70\times28$ and $80\times32(\Delta z = 10^{-6}\sim3.2\times10^{-5})$ are estimated to be within 1.08% at $z=0.1$. Table 2 gives the value of Nu by using $M\times N(\Delta z) = 90\times12$ and $120\times16(\Delta z = 10^{-6}\sim3.2\times10^{-5})$ for case 2 with $\mathrm{Pr}=0.7$, $\mathrm{Ra}=10^5$, and $\gamma=15$. It is noted in Table 2 that the difference in the local Nusselt number by using 90×12 and $120\times16(\Delta z = 10^{-6}\sim3.2\times10^{-5})$ grids is always less than 5%.

Table 1 Numerical experiment on mesh size ($M \times N$) and axial step size (Δz) for case 1 with $\gamma = 10$, Pr = 0.7, and Ra = 10^5

$M \times N$ (Δz) \ Nu \ z	0.002	0.010	0.050	0.100	0.300
70×28 ($1 \times 10^{-6} \sim 3.2 \times 10^{-5}$)	9.5944	6.2843	7.5992	10.9112	11.4620
70×28 ($2 \times 10^{-6} \sim 6.4 \times 10^{-5}$)	9.5914	6.3001	7.6421	10.8655	11.4118
80×32 ($1 \times 10^{-6} \sim 3.2 \times 10^{-5}$)	9.5741	6.2823	7.5598	10.7936	11.5785

Table 2 Numerical experiment on mesh size ($M \times N$) and axial step size (Δz) for case 2 with $\gamma = 15$, Pr = 0.7, and Ra = 10^5

$M \times N$ (Δz) \ Nu \ z	0.002	0.010	0.050	0.100	0.300
90×12 ($1 \times 10^{-6} \sim 3.2 \times 10^{-5}$)	9.5414	6.1857	5.9140	7.3593	4.6408
90×12 ($2 \times 10^{-6} \sim 6.4 \times 10^{-5}$)	9.5391	6.1864	5.9088	7.3207	4.5756
120×16 ($1 \times 10^{-6} \sim 3.2 \times 10^{-5}$)	9.6491	6.2185	5.6324	7.2099	4.6105

Table 3 Numerical experiment on mesh size ($M \times N$) and axial step size (Δz) for case 3 with $\gamma = 10$, Pr = 0.7, and Ra = 10^5

$M \times N$ (Δz) \ Nu \ z	0.002	0.010	0.050	0.100	0.033
60×12 ($1 \times 10^{-6} \sim 3.2 \times 10^{-5}$)	9.5337	6.8647	6.2976	6.0532	5.8984
60×12 ($2 \times 10^{-6} \sim 6.4 \times 10^{-5}$)	9.5256	6.8669	6.3016	6.0653	5.9014
80×16 ($1 \times 10^{-6} \sim 3.2 \times 10^{-5}$)	9.5902	6.8506	6.3119	6.0692	5.9149

However, the 90×12 meshes are too coarse to provide grid-independent results. Calculations for a finer mesh size were precluded by computer time requirements. For case 3 with $\gamma = 15$, Ra = 10^5, and Pr = 0.7, the numerical experiment, shown in Table 3, shows that the maximum deviation of Nu is always less than 0.7%. Therefore, the grids, $M \times N(\Delta z) = 60 \times 12(\Delta z = 10^{-6} \sim 3.2 \times 10^{-5})$, are suitable for case 3.

The heat transfer characteristics in the thermal entrance region of rectangular channels are usually presented by the spanwise average local Nusselt number Nu at each axial position. The variations of Nu versus Rayleigh number and axial distance z are shown in Figures 2–4 for cases 1–3 with $\gamma = 10$, 10 and 15, 10 and 15 and Pr = 0.7, 0.7 and 5, 0.7, respectively. An overall inspection of Figures 2–4 discloses that the buoyancy effect is negligible up to a certain axial distance and that this axial distance depends mainly on the magnitude of the Rayleigh number: the greater is Ra, the shorter is the distance. In Figure 2, the local Nusselt number along the top wall is zero in the initial entrance region. But as the flow goes downstream, the Nu along the top surface increases and then approaches that along the bottom surface. It is noteworthy that the asymptotic Nu in the downstream region exhibited an oscillatory phenomenon for Ra > 6×10^4. This confirms that the mixed convection flow would become unstable as Ra is high.[16] But for cases 2 and 3 (in Figures 3 and 4), the Nu, after reaching minimum and then maximum values for some curves, gradually approach the asymptotic values when the fully developed conditions are reached. The occurrence of maximum local Nusselt number for the cases with high Ra is closely related to the appearance of local maximum secondary flow intensity.[18] For Ra = 2×10^5 in Figures 3a and 3b, a larger value of z for air (Pr = 0.7) is needed for the secondary flow to occupy the entire spanwise direction under fixed aspect ratio, and the peak enhancement for air is approximately 19% (as $\gamma = 10$) and 6% (as $\gamma = 15$) less than that for water (Pr = 5). The discrepancy between the peak value of Nu for air and that for water decreases with the decrease in Ra and the increase in γ. It is also noted in Figures 3 and 4 that the thermal entrance length decreases with the increase in Ra.

It has been noted in the literature review that several kinds of criteria have been suggested for the onset of thermal instability. In experimental studies, a criterion based on flow visualization with an injection of dye was usually used.[6,7,10] A criterion based on the first longitudinal station at which heat transfer enhancement begins to deviate sharply from a gradual increase with the longitudinal coordinate was also used.[11] Since where and how the dye ascends from the plates or heat transfer enhancement increases sharply is directly caused by a finite amplitude of buoyancy effect, the criterion based on 2% deviation of local Nusselt number from that of classical Graetz theory is used in the present work. This criterion was also used by Ou et al.[12] to study the onset of the thermal instability. The comparison of present theoretical results with existing theoretical and experimental results for onset of thermal instability in the

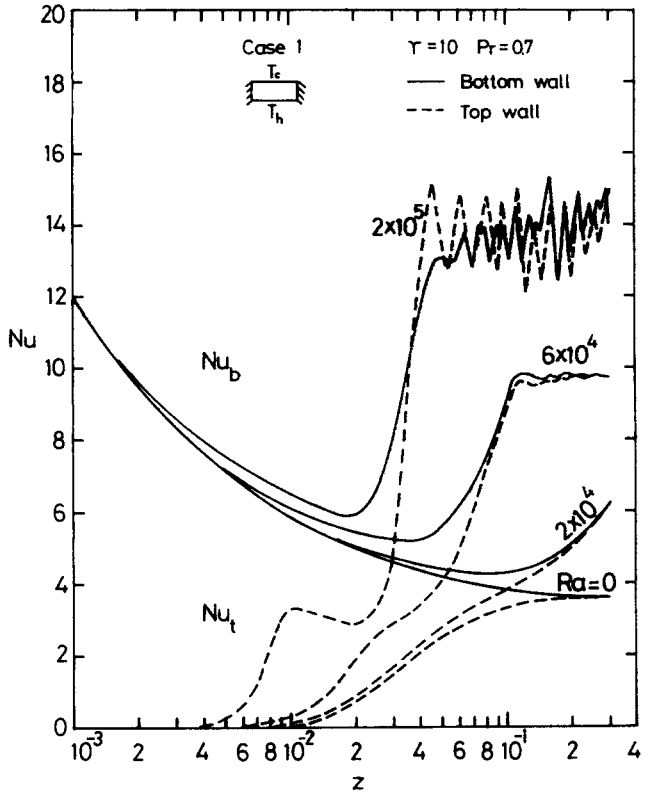

Figure 2 Effects of the Rayleigh number on bottom-plate and top-plate Nusselt numbers for case 1 with Pr=0.7 and $\gamma=10$

horizontal rectangular channels is shown in Figure 5. The numerical results of Ou et al.[12] correspond to flow of a large Prandtl number fluid in an isothermal channel of $\gamma=2$, while the experimental results of Hwang and Liu[6] and Kamotani and Ostrach[8] correspond to air flow in the thermal entrance region of horizontal parallel-plate channels heated from below and isothermally cooled at the top plate with aspect ratios, say about 15 and 17, respectively. To facilitate the comparison, the numerical results of this study were converted from a Rayleigh number and axial distance based on equivalent hydraulic diameter to a critical Rayleigh number Ra_c and axial distance z_c based on the height (b) of the channel.

$$Ra_c=[(1+1/\gamma)^3/8]Ra \tag{13}$$

$$z_c=[2/(1+1/\gamma)]z \tag{14}$$

As shown in Figure 5, the present predictions of the onset of thermal instability based on the 2% deviation from the Graetz theory show a decreasing deviation of these results from the previous experimental results when $Ra_c \leqq 8\times10^3$ and $Ra_c > 1.5\times10^4$. In addition, the present results approach those of the previous experimental study when the aspect ratio becomes large.

To ascertain the effects of Prandtl number, aspect ratio, and side-wall heating on thermal instability, it is of interest to compare the results of the present and previous predictions for three kinds of thermal boundary conditions with Pr=0.7, 5, 100 and $\gamma=2$, 10, and 15. The results in Figure 5 show that for cases 1 and 2, the onset of thermal instability is only slightly earlier for $\gamma=10$ than for $\gamma=15$ under fixed Prandtl number and thermal boundary conditions. But, for case 3, it is always rather earlier for $\gamma=10$ than for $\gamma=15$. This demonstrates that

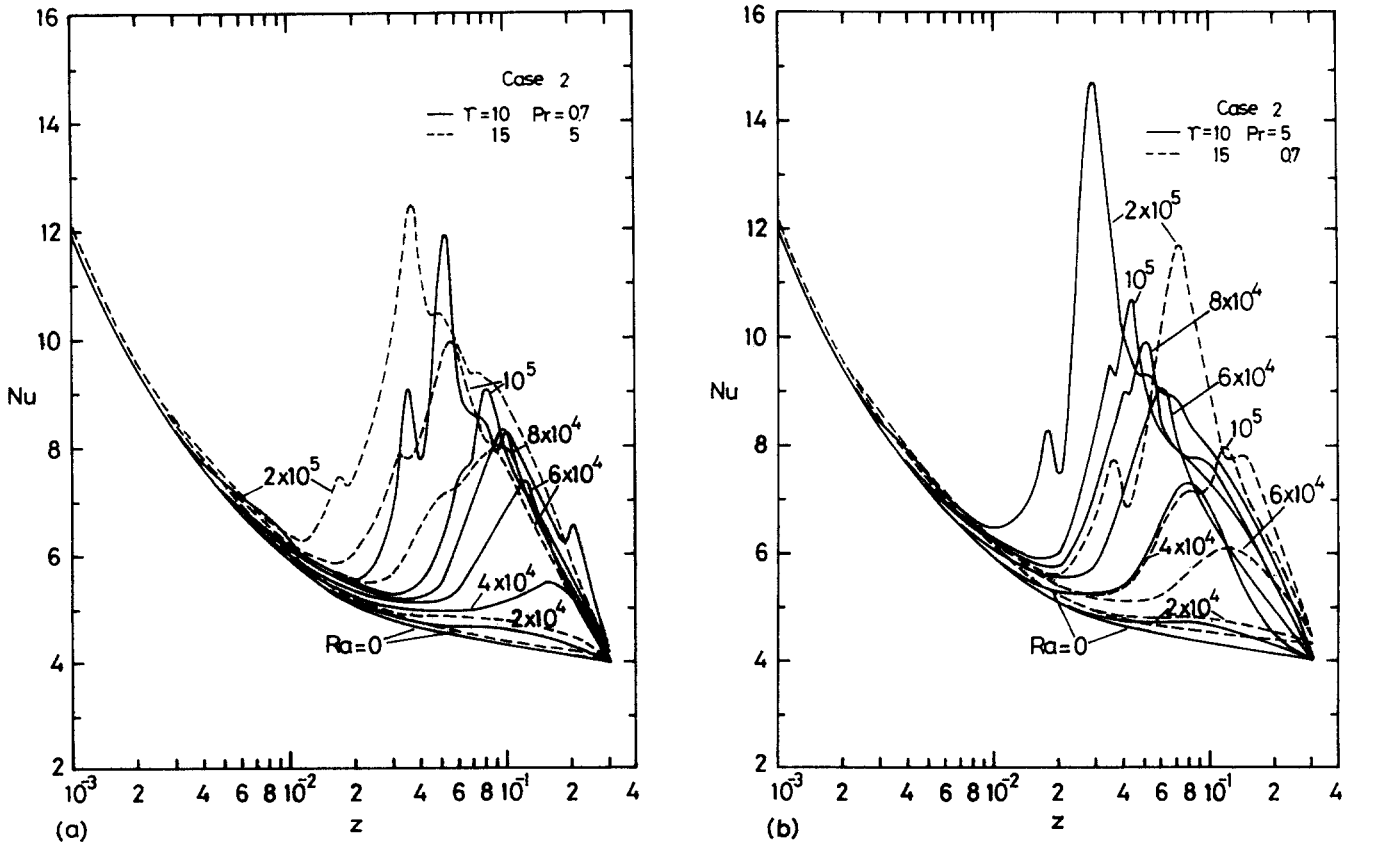

Figure 3 Effects of the Rayleigh number on the local Nusselt number for case 2 with (a) $\gamma=10$, 15 and Pr=0.7, 5 and (b) $\gamma=10$, 15 and Pr=5, 0.7

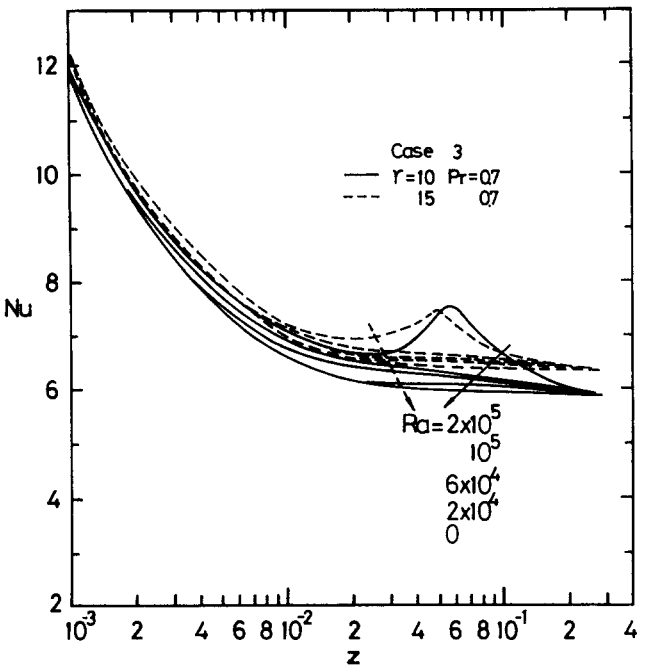

Figure 4 Effect of Rayleigh number on local Nusselt number for case 3 with $\gamma=10$, 15 and $Pr=0.7$

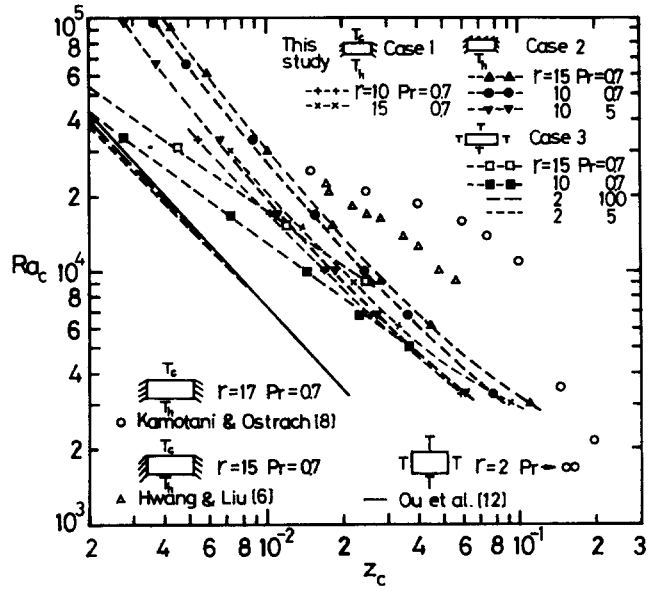

Figure 5 Comparison between the results based on a 2% departure and previous results for onset of thermal instability

the effect of aspect ratio on the thermal stability is not pronounced for cases 1 and 2 but is significant for case 3. The results for case 3 with $\gamma=2$ and $Pr=5$ and 100, exhibiting an excellent agreement with those of large Pr ($Pr\to\infty$) by Ou et al.,[12] show a significantly earlier onset. This implies that the effects of various Pr are very small under small aspect ratio and fixed thermal boundary conditions. This phenomenon is due to the heated side-wall effect, which is more significant when aspect ratio is small. The side walls induce a strong secondary flow in the region near the side walls (as shown in Ou et al.[12]) and make the onset of instability occur earlier. Furthermore, in the bottom-heated situation (case 2), the results for $Pr=5$ show earlier onset of instability than that of $Pr=0.7$ for a fixed aspect ratio. This is ascribed to the fact that the side-wall effect is insignificant and the air is slightly more stable than water.[11] Additionally, the comparison among the results of these three cases indicates that the onset of instability is earlier for case 3 than cases 1 and 2, especially for high Ra. This phenomenon is due to the fact that the strength of the buoyancy effects, which can enhance the secondary flow induced by a thermal instability due to bottom heating, increases more quickly with the increase in Rayleigh number near the heated side wall as compared to the adiabatic wall. From the foregoing illustration and discussion, we may conclude that the combined effects of aspect ratio, Prandtl number, and heated side wall are the reason why the results of Ou et al.,[12] corresponding to an isothermal channel with $\gamma=2$ and $Pr\to\infty$, show a much earlier onset of instability when compared with the experimental results of air flow in bottom-heated and large aspect ratio channels.[6,8]

The effects of another criterion, based on the location of local minimum Nu, on the analytical prediction of the onset of thermal instability is also considered for comparison. The sharp decline of Nusselt number in the entrance region for Graetz theory ($Ra=0$) is known to be the entrance effect due to the axial convective term only, and mixed-convection results deviate from forced-convection behavior due to the free-convection effect inducing an initiation of secondary flow in the corner. These two effects eventually balance out and the local minimum Nusselt number appears at some downstream location. Subsequently, the free-convection effect dominates over the entrance effect and the Nusselt number increases sharply, which indicates that the onset of thermally driven secondary flow is pronounced, until the maximum value for Nu is attained, due to secondary flow development over the entire spanwise direction. This is the reason why the criterion based on the local minimum Nusselt number was chosen for comparison in this study. Results based on this criterion (Figure 6) show an over-prediction compared with those of experimental works by Hwang and Liu[6] and Kamotani and Ostrach[8] when $Ra_c \geqq 2\times10^4$, but it reveals a very good agreement when $Ra_c < 2\times10^4$. Also found in Figure 5 is that the effects of aspect ratio on the thermal instability can be ignored under fixed Pr for cases 1 and 2, while for case 3 those effects become significant.

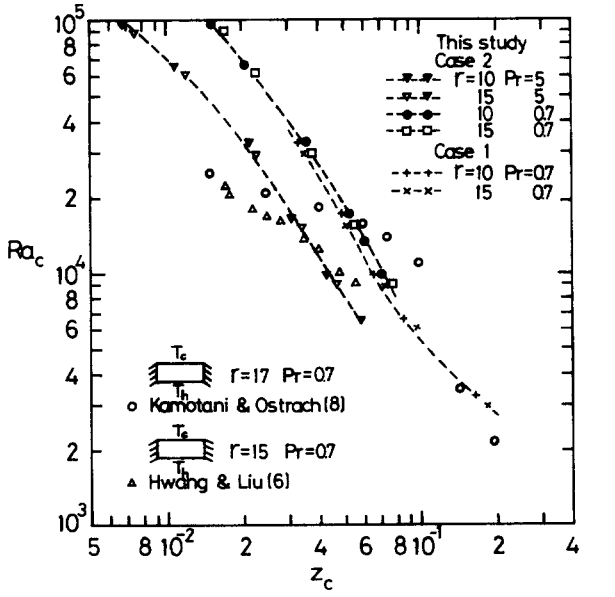

Figure 6 Comparison between the results based on the minimum Nusselt number and previous experimental results for onset of thermal instability

Comparing the results in Figure 6 for cases 1 and 2, it is clear that the influence of the cooled top wall on the thermal instability is very small, and this is consistent with the results of Incropera et al.[9] and Incropera and Schutt.[16] Comparing the results in Figure 6 and those in Figure 5, it is found that the predicted results are different between these two criteria. However, the streamwise distance to the onset of instability based on the minimum Nusselt number (Figure 6) is certainly expected to be larger than that defined by a 2% departure (Figure 5) when $Ra_c \geqq 2 \times 10^4$.

Concluding remarks

The onset of thermal instability in the thermal entrance region of horizontal rectangular ducts has been studied. In this work, two different instability criteria have been used to mark the onset point. The predicted results based on a 2% departure show an overall reasonable agreement with those of experimental works,[6,8] while the predicted results based on the minimum Nusselt number show a better agreement with the experimental data only in a narrow range ($Ra_c < 2 \times 10^4$).

The results based on a 2% departure (Figure 5) show that the thermal instability is only slightly affected by the change of Prandtl number for case 3 with small aspect ratio situations ($\gamma = 2$), but for large aspect ratio conditions ($\gamma = 10$, 15) the effects of the Prandtl number for cases 2 and 3 on the instability are significant. The influence of the variation of aspect ratio on thermal instability under a fixed Prandtl number is only pronounced for case 3.

The results based on the minimum Nusselt number (Figure 6) show an overprediction compared with those of the previous experimental works when $Ra_c \geqq 2 \times 10^4$, as well as showing a good agreement when $Ra_c < 2 \times 10^4$. The results also indicate that the cooled top-wall boundary condition (case 1) would slightly affect the thermal instability under a fixed Prandtl number. The change of aspect ratio does not influence the onset of thermal instability for cases 1 and 2 under fixed Prandtl numbers. On the contrary, under fixed aspect ratio conditions, the results for air ($Pr = 0.7$) are more stable than those for water ($Pr = 5$).

Acknowledgment

The authors would like to thank the National Science Council of The Republic of China for its support of the present work through project NSC79-0401-E008-01.

References

1 Mori, Y. and Uchida, Y. Forced convective heat transfer between horizontal flat plates. *Int. J. Heat Mass Transfer*, 1966, **9**, 803–817

2 Nakayama, W., Hwang, G. J., and Cheng, K. C. Thermal instability in plane Poiseuille flow. *ASME J. Heat Transfer*, 1970, **92**, 61–68

3 Hwang, G. J. and Cheng, K. C. Convective instability in the thermal entrance region of a horizontal parallel plate channel heated from below. *ASME J. Heat Transfer*, 1973, **95**, 72–77

4 Wu, R. S. and Cheng, K. C. Thermal instability of Blasius flow along horizontal plates. *Int. J. Heat Mass Transfer*, 1976, **19**, 907–913

5 Akiyama, M., Hwang, G. J., and Cheng, K. C. Experiments on the onset of longitudinal vortices in laminar forced convection between horizontal plates. *ASME J. Heat Transfer*, 1971, **93**, 335–341

6 Hwang, G. J. and Liu, C. L. An experimental study of convective instability in the thermal entrance region of a horizontal parallel-plate channel heated from below. *Can. J. Chem. Eng.*, 1976, **54**, 521–525

7 Kamotani, Y., Ostrach, S., and Miao, H. Convective heat transfer augmentation by means of thermal instability. *ASME J. Heat Transfer*, 1979, **101**, 222–226

8 Kamotani, Y. and Ostrach, S. Effect of thermal instability on thermally developing laminar channel flow. *ASME J. Heat Transfer*, 1976, **98**, 62–66

9 Incropera, F. P., Knox, A. L., and Schutt, J. A. Onset of thermally driven secondary flow in horizontal rectangular ducts. *Proc. 8th Int. Heat Transfer Conf.*, Hemisphere, Washington, DC, 1986, **3**, 1395–1400

10 Osborne, D. G. and Incropera, F. P. Laminar mixed convective heat transfer for flow between horizontal parallel plates with asymmetric heating. *Int. J. Heat Mass Transfer*, 1985, **28**, 207–217

11 Maughan, J. R. and Incropera, F. P. Experiments on mixed convection heat transfer for airflow in a horizontal and inclined channel. *Int. J. Heat Mass Transfer*, 1987, **30**, 1307–1318

12 Ou, J. W., Cheng, K. C., and Lin, R. C. Natural convection effect on Graetz problem in horizontal rectangular channels with uniform wall temperature for large Pr. *Int. J. Heat Mass Transfer*, 1974, **17**, 835–843

13 Cheng, K. C., Hong, S. W., and Hwang, G. J. Buoyancy effect on laminar heat transfer in the thermal entrance region of rectangular channels with uniform wall heat flux for large Prandtl number fluids. *Int. J. Heat Mass Transfer*, 1972, **17**, 1819–1836

14 Ramakrishna, K., Rubin, S. G., and Khosla, P. K. Laminar natural convection along vertical square ducts. *Numer. Heat Transfer*, 1982, **5**, 59–79

15 Abou-Ellail, M. M. M. and Morcos, S. M. Buoyancy effects in the entrance region of horizontal rectangular channels. *ASME J. Heat Transfer*, 1983, **105**, 152–159

16 Incropera, F. P. and Schutt, J. A. Numerical simulation of laminar mixed convection in the thermal entrance region of horizontal rectangular ducts. *Numer. Heat Transfer*, 1985, **8**, 707–729

17 Mahaney, H. V., Incropera, F. P., and Ramadhyani, S. Development of laminar mixed convection in a horizontal rectangular duct with uniform bottom heating. *Numer. Heat Transfer*, 1987, **12**, 137–155

18 Chou, F. C. and Hwang, G. J. Vorticity-method for Graetz problem with the effect of natural convection in a horizontal rectangular channel with uniform wall heat flux. *ASME J. Heat Transfer*, 1987, **109**, 704–710

19 Cheng, K. C. and Ou, J. W. Convective instability and finite amplitude convection in the thermal entrance region of horizontal rectangular channels heated from below. *Proc. 7th Int. Heat Transfer Conf.*, Hemisphere, Washington, DC, 1982, **2**, 189–194

20 Patankar, S. V. and Spalding, D. B. A calculation procedure for heat, mass and momentum transfer in three-dimensional parabolic flow. *Int. J. Heat Mass Transfer*, 1972, **15**, 1787–1806

21 Ou, J. W. and Cheng, K. C. Natural convection effects on Graetz problem in horizontal isothermal tubes. *Int. J. Heat Mass Transfer*, 1977, **20**, 953–960